Introducing LAB60: A 1/60° NEMO 3.6 numerical simulation of the Labrador Sea

Clark Pennelly[1*] and Paul G. Myers[1]

[1]1-26 Earth Sciences Building, University of Alberta, Edmonton, Alberta, Canada, T6G 2E3

[*]*Correspondence to*: Clark Pennelly (pennelly@ualberta.ca)

Abstract

A high-resolution coupled ocean-sea ice model is set up within the Labrador Sea. With a horizontal resolution of 1/60°, this simulation is capable of resolving the multitude of eddies which transport heat and freshwater into the interior of the Labrador Sea. These fluxes strongly govern the overall stratification, deep convection, restratification, and production of Labrador Sea Water. Our regional configuration spans the full North Atlantic and Arctic, while the high resolution is only applied in smaller nested domains within the North Atlantic and Labrador Sea. Using nesting reduces computational costs and allows for a long simulation from 2002 to the near-present time. Three passive tracers are also included: Greenland runoff, Labrador Sea Water produced during convection, and Irminger Water which enters the Labrador Sea along Greenland. We describe the configuration setup and compare against similarly forced lower-resolution simulations to better describe how horizontal resolution impacts the representation of the Labrador Sea in the model.

1. Introduction

The Labrador Sea, between Canada and Greenland, plays a crucial role in the climate system. Situated between the Canadian Arctic and the North Atlantic, multiple current systems influence this deep basin. Cold and fresh Arctic water flows south through Fram Strait along Greenland (de Steur et al., 2009), producing the East Greenland Current (EGC). The EGC flows to the southern tip of Greenland, merging with warm and salty Irminger Water to become the West Greenland Current (WGC) before flowing northwards along the western coast (Fratantoni and Pickart, 2007). The WGC flows cyclonically around the Labrador Sea as well as into Baffin Bay. Significant amounts of freshwater are supplied to this current system from both Davis (Cuny et al., 2005; Curry et al., 2011; Curry et al., 2014) and Hudson Strait (Straneo and Saucier,

2008) as it travels around the Labrador Sea. The current system is called the Labrador Current where it merges with the outflow from Hudson Strait (Lazier and Wright, 1993). The Labrador Current travels southwards along the eastern coast of North America eventually leaving the Labrador Sea.

Numerous eddies are generated throughout the Labrador Sea, both from high lateral density gradients which exist during the convection season (Frajka-Williams et al., 2014) as well as from baroclinic and barotropic instabilities that occur within the boundary currents (Chanut et al., 2008; Gelderloos et al., 2011). The continental slope along the west coast of Greenland has a pronounced change in topography that induces instability of the current system, generating eddies (de Jong et al., 2016). These eddies, known as Irminger Rings, contain a significant amount of freshwater at the surface as well as subsurface heat. Irminger Rings (15-30km radius) typically travel southwestwards into the interior of the Labrador Sea and have a lifespan of up to two years (Lilly et al., 2003). Eddies generated along the Labrador Coast also contain a significant amount of freshwater (Schmidt and Send, 2007; McGeehan and Maslowski, 2011; Pennelly et al., 2019). Regardless of where they are produced, these boundary current eddies often export their properties towards the centre of the basin (Pennelly et al., 2019), influencing the deep convection which occurs. Convective eddies are generated from baroclinic instability which arises from large horizontal density gradients during the convective season (Marshall and Schott, 1999). Convective eddies are much smaller with a radius between 5 and 18 km (Lilly et al., 2003). These eddies are less studied than the other eddy types, partly due to a lack of observations (Lilly et al., 2003) as well as their small size which requires high-resolution models to adequately resolve. Research into the role of each of the above eddies and their role in restratifying the Labrador Sea is still ongoing; there is no consensus on which eddy may be more important, though many have narrowed it down to Irminger Rings and convective eddies (Chanut et al., 2008; Gelderloos et al., 2011; Rieck et al., 2019).

Deep convection is a rather rare occurrence, only known to occur at a few places in the ocean. The reason so few places exist is the stringent criteria to produce deep convection: weak stratification that can be enhanced via isopycnal doming as a result of cyclonic circulation, and

intense air-sea buoyancy loss (Lab Sea Group, 1998; Marshall and Schott, 1999). Cyclonic circulation and the lateral input of salty Irminger Water helps keep the Labrador Sea weakly stratified. Furthermore, the Labrador Sea experiences strong heat loss during the winter period due to the very cold mid-latitude cyclones which frequent the region (Schulze et al., 2016). The overlying cold and dry air forces a significant flux of heat from the ocean to the atmosphere. This loss of heat promotes the surface layer to increase in density, overturning the weakly stratified water column such that the mixed layer can exceed 2000m in depth (Yashayaev, 2007), producing a thick uniform water mass known as Labrador Sea Water (LSW).

Once the convective winter ends, the Labrador Sea quickly restratifies itself within 2-3 months (Lilly et al., 1999), primarily due to large horizontal density gradients that form convective eddies (Lilly et al., 2003; Rieck et al., 2019) as a result of the deep convection period (Frajka-Williams et al., 2014). The boundary currents continuously shed eddies with relatively buoyant water towards the interior Labrador Sea (Straneo, 2006), increasing stratification. This occurs along the west Greenland and Labrador coasts, though research suggests that the former supplies more freshwater (Myers, 2005; Schmidt and Send, 2007; McGeehan and Maslowski, 2011; Pennelly et al., 2019).

LSW is exported out of the Labrador Sea primarily by the Deep Western Boundary Current (Kieke et al., 2009), though it also spreads eastwards at a slower rate. While LSW is the lightest component within the Deep Western Boundary Current, it is one of the water masses which make up the lower limb of the Atlantic Meridional Overturning Circulation (AMOC). As the overturning circulation transports a significant amount of heat and dissolved gasses between the equator and polar regions, changes in the production of deepwater can influence the overturning circulation and ultimately the climate (Bryden et al., 2005). With polar amplification driven by the positive ice-albedo feedback loop, additional freshwater from melted ice enters the EGC and WGC (Bamber et al., 2012). The Labrador Sea is experiencing an increase in freshwater that can be capable of capping convection and preventing LSW from being formed, ultimately reducing the AMOC strength (Böning et al., 2016). However, a non-local increase in the surface freshwater flux may promote AMOC strengthening (Cael and Jansen, 2020) or compensate the local effects of additional freshwater (Latif et al., 2000). Long

climate simulations allow investigation into any AMOC regime shifts that shorter, higher-resolution simulations may miss. With such different conclusions, freshwater's influence on the AMOC is not fully known and may vary at different convection regions.

While satellite altimetry provides a wealth of information including sea surface height anomalies, geostrophic currents, and waves, hydrographic cruises within the Labrador Sea are often limited to the restratification period when the Labrador Sea is more hospitable for scientific operations. Argo floats, autonomous drifting profilers which can sample down to 2000m, have become a popular instrument to acquire in-situ data. However, they still lack coverage within the Labrador Sea which can experience deep convection below their sampling depth (Yashayaev, 2007). Numerical modelling is a useful tool to explore this data-sparse region, though it has its limits. Simulations within the Labrador Sea often experience a drift in model data, producing a Labrador Sea which slowly increases in salinity, and thus density (Treguier et al., 2005; Rattan et al., 2010). Coarse-resolution simulations suffer even further, often overproducing the spatial area of deep convection (Courtois et al., 2017), primarily as a result of not resolving important small-scale features including eddies. These eddies supply the Labrador Sea with significant heat (Gelderloos et al., 2011) and freshwater fluxes (Hátún et al., 2007), both strongly impact the stratification, convection, and production of deep water. Increased horizontal resolution helps produce these eddies and their important fluxes into the interior of the Labrador Sea but numerical drift still is present within high-resolution simulations, albeit reduced in severity (Marzocchi et al., 2015).

Numerous high-resolution simulations have been carried out within the North Atlantic. VIKING20X (Rieck et al., 2019), and its predecessor VIKING20, are global 1/4° simulations which have a high-resolution 1/20° nest. VIKING20X is a multi-decade simulation which is capable of resolving eddies within the Labrador Sea. However, simulations with 1/20° horizontal resolution may not resolve sub-mesoscale processes (Su et al., 2018) that can impact stratification by carrying heat and freshwater; higher-resolution is needed. The 1/50° HYCOM (Chassignet and Xu, 2017), 1/60° NATL60 (Fresnay et al., 2018) and eNATL60 (Le Sommer et al., in prep) provide great insights on the importance of resolving eddies. However, computational expense with such high-resolution simulations is very high, both in computer time and operational costs. This

often forces higher-resolution simulations to have a reduced length, perhaps only a few years. The Labrador Sea experiences significant interannual variability (Fischer et al., 2010) and such short simulations may completely miss any connection between LSW production and changes in the AMOC. As such, any high-resolution simulation which is capable of resolving the fine scale features within the Labrador Sea should be carried out for many years to further understand the climate system. Resolving the full North Atlantic at high resolution (1/60°) and carrying out a simulation for longer than 10 years would currently be extremely expensive; the above 1/60° simulations are 5 or so years in length. However, one can incorporate nested domains to increase horizontal resolution with a relatively minor increase in computing cost.

To simulate the Labrador Sea as accurately as possible, we set up a complex numerical configuration which achieves very high resolution within the Labrador Sea while keeping computing costs low such that we will produce over 15 years of simulated data. This simulation will be kept up to near-present time, lagged a few months depending on the availability of forcing data. The high resolution allows for explicit representation of eddies which are crucial to controlling the stratification within the region. We will first describe the model configuration in detail and then compare against similarly-forced lower-resolution simulations to understand how changes in horizontal resolution impacts model results in the Labrador Sea.

2. Methods

The numerical model used for our high-resolution simulation is the Nucleus for European Modelling of the Ocean (NEMO; Madec, 2008), version 3.6, which is coupled to a sea-ice model, LIM2 (Fichefet and Maqueda, 1997). The 1/4° Arctic Northern Hemisphere Atlantic configuration (ANHA4; Fig 1a) is used and includes a double nest via the Adaptive Grid Refinement in FORTRAN package (AGRIF; Debreu et al., 2008). The AGRIF software allows for high-resolution nests to communicate along their boundaries, passing information back and forth between domains. The parent ANHA4 domain extends from Bering Strait, though the Arctic and North Atlantic, to 20°S in the South Atlantic. The parent domain's nest uses a spatial and temporal refinement factor of three, bringing resolution to 1/12° and the time step to 240s (Table 1) in the North Atlantic Sub Polar Gyre domain (SPG12; Fig 1b). An ANHA4 configuration

with a SPG12 nest has been evaluated before by investigating how model resolution influences Labrador Sea Water formation (Garcia-Quintana et al., 2019) as well as eddy formation and eddy fluxes in the North Atlantic Current (Müller et al., 2017; Müller et al., 2019). Another nest is implemented within the SPG12 domain, using a spatial and temporal refinement of five, increasing the horizontal resolution from 1/12° to 1/60° and reducing the time step to 48s within the Labrador Sea (LAB60; Fig 1c). All nests allow two-way communication such that the parent domain supplies boundary conditions while the daughter domain returns interpolated values to all associated parent grid points. All domains have different horizontal grid spacing but they share the same vertical grid which is set to 75 geopotential levels (Fig. 1d) using partial steps (Barnier et al., 2006). This simulation involves three domains (ANHA4, SPG12, and LAB60) although we primarily discuss what occurs within the 1/60° nest.

A total variance dissipation scheme (Zalesak, 1979) was used in all domains to calculate horizontal advection. A Laplacian operator was used to compute lateral diffusion in all domains, while a bi-laplacian operator was used for lateral momentum mixing. As some model parameters are grid-scale dependent, Table 1 displays these settings. As lateral boundary conditions have been shown to be very important at producing Irminger Rings in high-resolution simulations (Rieck et al. 2019), we used no-slip lateral boundary conditions within the LAB60 domain while the other domains had free-slip conditions. Model mixed layer depths were calculated via the vertical gradient in temperature and salinity (Holte and Talley, 2009) as opposed to a 0.01 kg m^{-3} change in potential density between the surface and the bottom of the mixed layer; the latter method can produce deeper mixed layers than observations suggest (Courtois et al., 2017). Settings not listed in Table 1 indicate that all domains have an identical value or option; some of these important settings are shown in Table 2.

Model bathymetry was interpolated from the 1/60° ETOPO GEBCO dataset (Amante and Eakins, 2009) to each domain's grid and bathymetric smoothing along nest boundaries was carried out in order to conserve volume where the parent domain supplies boundary conditions to the daughter domain. All domains were initialized from GLORYS1v1 (Ferry et al., 2009), a global reanalysis ocean simulation, at the beginning of 2002. Monthly open boundary conditions (3D T, S, U, V, and 2D SSH and ice values) across Bering Strait and 20° S were

supplied to the ANHA4 domain. These boundary conditions were linearly interpolated from monthly values, overriding the values within the boundary without the use of a sponge layer. Runoff was supplied via Dai et al. (2009) while we also included Greenland runoff as estimated from a surface mass-balance model (Bamber et al., 2012). Without an iceberg model functioning with the AGRIF software, we treated all solid runoff as a liquid, thus capturing the full freshwater mass at the cost of accuracy in the spatial and temporal placement of freshwater emitted from icebergs.

Precipitation, shortwave radiation, downward longwave radiation, 2 meter specific humidity, 2 meter temperature, 10 meter meridional and 10 meter zonal winds originally were supplied from the Canadian Meteorological Centre's Global Deterministic Prediction System's Reforecast product (CGRF; Smith et al., 2014). While high in temporal (hourly) and spatial resolution (33 km in the Labrador Sea), we found the air-sea fluxes were slightly too weak to sustain deep convection after 2010. Rather than start completely over, we switched the atmospheric forcing in 2007 (Fig. 2) when LAB60's mixed layer was still similar to observations. Starting on 1 Jan 2007, we used the DRAKKAR Forcing Set 5.2 (DFS; Dussin et al., 2016). DFS supplies data at 3 hour increments for wind, temperature, and humidity, while precipitation and radiation are daily. DFS has a spatial resolution which is approximately 45 km within the Labrador Sea. Our own analysis of the CGRF data showed a 2002-2015 average yearly heat loss of 47 W m^{-2} from the interior Labrador Sea while DFS removed 53 W m^{-2} (Pennelly and Myers, submitted). Increasing the horizontal resolution likely increased the horizontal buoyancy fluxes and rendered the CGRF's air-sea heat loss, which was appropriate in our ANHA4 and ANHA12 configurations, inadequate. The decision to swap to DFS was based on its greater heat loss, promoting a better mixed layer depth throughout the Labrador Sea, though a different forcing product will eventually be needed as DFS does not currently extend past 2017. Supplemental Fig. 1 depicts the difference in mixed layer depth between the LAB60 simulation forced by CGRF, when forced with CGRF through 2007 and then forced by DFS, as well as what ARGO observations suggest. The weaker air-sea heat loss as forced by the CGRF product leaves the mixed layer with little interannual variability that doesn't compare well with observations.

Early testing showed that adding passive tracers increases the computing resources required by about 20% per passive tracer. To keep the simulation from requiring too many resources, we limited LAB60 to three passive tracers:

1. Liquid runoff from Greenland
2. Irminger Water (T> 3.5°C, S>34.88) which flows westward past Cape Farwell (Fig. 3b)
3. Labrador Sea Water (σ_θ>27.68 kg m^{-3}) formed within the mixed layer of the Labrador Sea (Fig. 3c)

Runoff from Greenland was included due to the importance of Greenland's freshwater contribution to changes within the Labrador Sea. Water mass definitions for Irminger Water and Labrador Sea Water were selected based on previous studies (i.e. Kieke et al., 2006; Myers et al., 2007). Note that there is no maximum density criteria given to our Labrador Sea Water tracer- the tracer is formed throughout the water column until it reaches the bottom of the mixed layer. Figure 3 illustrates both the source regions as well as the tracer extent as of 1 Jan 2010. While these water masses have been studied before (Kieke et al., 2006; Myers et al., 2007; Böning et al., 2016), there has been no attempt to use them as passive tracers at a resolution higher than 1/20° (Böning et al., 2016).

The LAB60 simulation originally started on the Graham cluster of Compute Canada. Other high-resolution simulations often use thousands of computer processors but our simulation could not run on more than 672 CPUs on this cluster as it would stall during domain construction. The years 2002-2007 were carried out on Graham, after which a new allocation on a different high performance Compute Canada cluster, Niagara, became available to us. The LAB60 simulation on Niagara did not suffer from the same issue as it did on Graham and we were able to use many more processors. Initial testing found a substantial increase in the number of days simulated per job submission when the number of CPUs was increased from 672 to 3000; tests using 4000 CPUs showed no further improvement. Thus, we carried out the remainder of the LAB60 simulation with 3000 CPUs. Each job submission required around 22 hours to carry out, providing 40 days of model output. The real time to finish each 40 day submission naturally varied across the year, increasing during winter which we attribute to the sea-ice model.

A spin-up period (Fig. 2) was required as the model quickly went unstable and crashed. We attribute this to the interpolation of the 1/12° GLORYS1v1 data onto the LAB60 grid; the resulting data were not smooth enough and numerical noise was generated, leading to model failure. To reduce this noise, a gradual spin-up procedure took place. First, we kept the numerical timestep very low (2s in LAB60) when the model was initialized. We also set the 1/60° nests' eddy viscosity and diffusivity values to be equal to those within the SPG12 nest. We gradually increased the timestep and reduced the viscosity and diffusivity values over the first year (2002) to what is within Table 1. Other than also increasing the timestep to stay in line with LAB60, no other values were changed across the coarser ANHA4 and SPG12 domains. To allow LAB60 to adjust to the final settings, we consider the 2003 year to be an adjustment year (Fig. 2).

To assess the validity of LAB60, model results were compared against AVISO satellite data (https://www.aviso.altimetry.fr/), specifically U/V geostrophic velocities which are derived from the sea surface height. Argo profiler data (http://www.argo.net/) was also used to assess the mixed layer. Bottle data from cruise 18HUD20080520, accessed from CCHDO (https://cchdo.ucsd.edu/cruise/18HU20080520) on 10 April 2018 was used to compare observations across the AR7W section.

3. Model Simulation Results

To understand what is gained by resolving the Labrador Sea at 1/60°, we compare the output of our LAB60 simulation with similarly forced ANHA simulations at both 1/4° (ANHA4) and 1/12° (ANHA12). The large-scale circulation (top 50m) is shown for our 3 simulations (Fig. 4) as well as AVISO geostrophic velocities. All simulations have greater speed within the West Greenland Current (ANHA4: up to 0.8; ANHA12: 0.8; LAB60: 0.6; AVISO: 0.4 m s^{-1}) and Labrador Current (ANHA4: up to 0.6; ANHA12: 0.6; LAB60: 0.4; AVISO: 0.4 m s^{-1}) as altimetry observations suggest slower speeds here. However, Lin et al., (2018) found maximum speed up to 0.74 m s^{-1} along the west coast of Greenland. Both the ANHA4 and ANHA12 configuration have larger values further up the western coast of Greenland, as well as connecting the West Greenland Current and the Labrador Current; features that do not occur in both LAB60 and observations.

As LAB60 and observations have less average speed occurring within these boundary currents, we suspect that all configurations have some large differences in eddy activity, particularly where these boundary currents are.

Eddy kinetic energy (EKE: $0.5(\overline{U_g'^2} + \overline{V_g'^2})$, Fig. 5) was calculated from geostrophic velocity anomaly based on the sea level anomaly (SLA) from the 2004-2013 mean state:

$$U_g' = -\frac{g}{f}\frac{SLA}{\Delta y}$$

$$V_g' = -\frac{g}{f}\frac{SLA}{\Delta x}$$

where g is the gravitational constant, *f* is the Coriolis parameter, and Δy and Δx are model grid length. Overbars indicate the 2004-2013 mean value while primed variables indicate a deviation from the mean state. AVISO observations were already supplied as geostrophic velocities.

High levels of EKE can be found along the west coast of Greenland (Fig. 5), extending into the interior of the basin around 62° N, as well as along the Labrador coast's shelf break. The path extending from the west coast of Greenland is mostly due to Irminger Rings which leave this coast and travel westward (Chanut et al., 2008). While the EKE extending from west Greenland enters the interior of the Labrador Sea, that which stems from the Labrador coast does not penetrate far into the interior. The ANHA4 simulation has low EKE along the west coast of Greenland (around 100 $cm^2\ s^{-2}$) and along the Labrador Coast's shelf break (10-30 $cm^2\ s^{-2}$). The ANHA12 simulation shows improvement, having much higher EKE extending from west Greenland (100-300 $cm^2\ s^{-2}$) however the EKE does not quite extend into the interior of the Labrador Sea but instead remains in the northern Labrador Sea. Furthermore, there is additional EKE along the Labrador shelf break (30-50 $cm^2\ s^{-2}$) compared against ANHA4. The LAB60 simulation shows further improvement as the EKE signature from the west Greenland coast is greater (100-1000 $cm^2\ s^{-2}$) and now enters into the interior of the Labrador Sea. A notable increase in EKE also occurs along the Labrador shelf break (100-200 $cm^2\ s^{-2}$) and within the interior Labrador Sea (10-100 $cm^2\ s^{-2}$). LAB60 matches well against observations along the west coast of Greenland and the Labrador shelf break (both above 1000 $cm^2\ s^{-2}$) as well as the interior Labrador Sea (10-100 $cm^2\ s^{-2}$). LAB60's higher interior EKE may be partially from convective eddies that are formed during the wintertime. However, LAB60 has lower EKE within

the Northwest Corner where ANHA4, ANHA12, and the observations exceed 1000 $cm^2\ s^{-2}$ over a wide area. LAB60 matches the spatial distribution albeit with reduced EKE.

The differences in the EKE field between these configurations identify that each simulation is resolving features of varying spatial scales. The ANHA4 simulation, with low EKE within the Labrador Sea, does not adequately resolve eddies in this region, as illustrated with a snapshot of normalized model relative vorticity (Fig. 6). However, the larger scale meanders within the North Atlantic Current are visible. ANHA12 shows a greater degree of mesoscale features (50 to 500 km), though distinct eddies within the Labrador Sea are also not resolved. LAB60 resolves eddies along both the west coast of Greenland as well as the Labrador Coast. A video showing LAB60's normalized relative vorticity is shown in Supplementary Video 1.

A few Irminger Rings are shown in Fig. 7, a snapshot in time from 26 July 2007. A newly spawned ring (Fig. 7c) shows very strong surface speeds (up 0.6 m s^{-1} for Ring A; Fig. 7a) while older eddies to the south have reduced speeds (up to 0.3 m s^{-1} for Ring B; Fig. 7a). To investigate the stratification strength, we calculate the amount of energy needed to produce a neutrally stratified column extending down to some reference depth, *h*. This proxy, called convective energy, is given by:

$$Convective\ energy(h) = \frac{g}{Area} \int \int \left[h\, \rho_\theta(h) - \int_0^h \rho_\theta(z)\, dz \right] dA$$

where *g* is the gravitational constant, *Area* is the total surface area over our region of interest (Fig. 1c), *h* is the reference depth (2000m used in this study), $\rho_\theta\ (z)$ and $\rho_\theta\ (h)$ are the potential density at each grid cell and the potential density of the grid cell at the reference depth, and *A* is the surface area of each grid cell. A strongly stratified column of water corresponds to a high convective energy value. A snapshot of convective energy (Fig. 7b) shows that most of these eddies have substantially higher amounts compared to the background Labrador Sea, suggesting that the cool and fresh WGC water, as well as warm and salty Irminger Water keep these eddies strongly stratified. However, these eddies age within the Labrador Sea, and while a new eddy has strong stratification (>3000 J m^{-3}), an eddy which has evolved over many months (Fig. 7d) has weaker stratification (about 2000 J m^{-3}). Older eddies may have very weak stratification as they may have experienced two convective winter periods of buoyancy

removal. This has been noted before, as Lilly et al. (2003) found aged Irminger Rings with a mixed layer that surpassed 1000m.

These differences in resolving the mesoscale (50 to 500 km) and sub-mesoscale (<50 km) processes within each simulation produced significant changes within the Labrador Sea as seen from modeled convective energy values as averaged from 2004-2013 (Fig. 8). Resolving few eddies, the ANHA4 simulation's interior Labrador Sea lacks the buoyancy flux and remains very weakly stratified across a wide region. The ANHA12 simulation partially resolves some mesoscale features and eddy fluxes from the Greenland coast which supplies buoyancy to the Northern Labrador Sea and has higher convective energy. Furthermore, the spatial extent of the weakly stratified region has shrunk and resides primarily within the Labrador Sea, as opposed to ANHA4 which spills out of the basin. LAB60, fully capable of resolving buoyant eddies from the Greenland and Labrador coast, as well as convective eddies, has a much stronger degree of stratification in the interior region. A visible path of strong stratification appears around 60°N along this coastline, eventually extending away from the coastline around 62°N. This path is consistent with the general path that simulated Irminger Rings take (Chanut et al., 2008). Supplemental Video 2 shows the convective energy of the LAB60 simulation from 2004 through the end of 2013.

The ANHA4 simulation experiences weaker stratification in the Labrador Sea than ANHA12 and LAB60, driving a deeper maximum mixed layer that also covers a larger spatial extent (Fig. 9). However, the maximum mixed layer depth as simulated by ANHA4 and ANHA12 greatly exceed what Argo observations suggest (Fig. 9d). ANHA12 has higher EKE within the WGC, supplying more buoyancy to the northern portion of the Labrador Sea, reducing both the vertical extent of the mixed layer as well as the spatial extent where the mixed layer is deeper than 1000m. LAB60 has higher EKE than ANHA12, and the vertical and spatial extent of deep mixing is reduced even further. LAB60's mixed layer is far more similar to what ARGO observations suggest, suggesting the additional eddy fluxes to be fairly accurate. The evolution of LAB60's mixed layer depth is shown in supplemental video 3 from 2004 through the end of 2013.

After the bottom of the mixed layer returns to the near-surface, a newly formed LSW mass is left behind. To account for density drift, we allow the LSW classification to evolve in time, unlike our LSW passive tracer. We calculated LSW density and thickness by binning by potential density, referenced to 1000 dbar, with bin lengths of 0.001 kg m^{-3}. This was carried out within the black outlined polygon in Fig 1c for each daily output file per year. The density bin which had the thickest layer across the year was set as the maximum density of LSW for that year. The minimum density was defined to be 0.02 kg m^{-3} less than the maximum density. Linear interpolation occurred between years to allow for a gradual shift in density to prevent staircase patterns from emerging. Large differences in both the density as well as the thickness are present between the simulations shown in Fig. 10. The ANHA4 and ANHA12 simulations have similar density values of LSW while the LAB60 simulation is less dense. While the interannual variability matches fairly well across all configurations, the density values suggested by LAB60 are closer to ARGO observations (32.34 to 32.36 kg m^{-3}; Yashayaev and Loder, 2016) during the same time period. We suspect the denser LSW formed by ANHA4 and ANHA12 is primarily attributed to the lack of buoyancy coming from Greenland. As similar air-sea heat losses should occur in all three configurations, the weaker stratification of ANHA4 and ANHA12 indicates that deep mixing is more likely producing not only a denser LSW layer, but also a thicker one. Yashayaev and Loder (2016) also investigated the thickness of LSW (their Fig. 8), and while our simulations do not quite capture the same interannual variability and amplitude suggested their analysis using ARGO profilers, LAB60 is far more accurate than the lower-resolution configurations.

All simulations encounter some degree of numerical drift within the Labrador Sea (Fig. 11), judging from the salt and heat content change as calculated between the surface and seafloor within the polygon in Figure 1 since 2004. ANHA4 experiences the largest drift in both salt and heat, helping us understand why LSW is so dense in this simulation. ANHA12 also experiences drift, though slightly less severe. LAB60 has a small but gradual increase in both salt and heat content although it is difficult to state if this is drift or simply interannual to decadal variability. Regardless of the cause, LAB60's change in both heat and salt content is very minimal compared against the lower-resolution simulations.

When compared against bottle data collected during a single hydrographic cruise across Atlantic Repeat Hydrography Line 7 West (AR7W; Fig 12), LAB60 is slightly warmer (about 0.25 °C) and saltier (about 0.05 kg m^{-3}) throughout the interior. This causes LAB60 to be slightly denser with isopycnals residing higher than observations during this cruise suggest. Observations were not carried out above Greenland's continental slope, although they show some presence of the warm core of the WGC which the model captures. Salinity values close to the Labrador coast compare well while LAB60 is slightly warmer (about 0.5 °C) above the continental shelf.

The three passive tracers implemented within the full LAB60 configuration (Fig. 3) show where Greenland runoff, Irminger Water, and Labrador Sea Water travel to. These tracers were selected because they either contain a significant amount of buoyant water compared to the Labrador Sea, or are produced via convection in the Labrador Sea. From this image on 1 Jan 2010, we see a large portion of Greenland's runoff (Fig. 3a) resides within Baffin Bay as well as along the Labrador Coast. Some of this tracer is present where the ocean depth is greater than 2000m. A few Irminger Rings are identifiable, due to their thicker freshwater cap, which are in water deeper than 3000m. Little exchange with the interior basin appears to occur along the Labrador Current until the vicinity of Flemish Cap, after which a significant portion of the tracer propagates eastward. Supplemental Video 4 shows this the evolution of this tracer from 2004 through the end of 2013.

Irminger Water (T>3.5°C, S> 34.88; Fig. 3b) which flows west past Cape Farwell, enters the interior Labrador Sea with the greatest amounts where the seafloor is at a depth between 2000 and 3000m. Similar as above, individual Irminger Rings are visible, containing a larger amount of Irminger Water than the surrounding water. This water mass also flows along the Labrador Coast until it is in the vicinity of Flemish Cap. Supplemental Video 5 shows this the evolution of this tracer from 2004 through the end of 2013.

Our Labrador Sea Water tracer (Fig. 3c) is traced where the mixed layer produces water with a potential density above 1027.68 kg m^{-3} within the black contour identified in the figure. This definition differs compared to our method of classifying LSW as we did not implement any FORTRAN code to detect and compensate for density drift of our simulation, instead sticking to

a strict density classification for this tracer. As this image was made at the start of the convection season, the current deep patch is a freshly produced layer that reaches up to 800m deep. After forming, LSW spreads southwards along the Labrador shelf break as well as to the southeast. Supplemental Video 6 shows this the evolution of this tracer from 2004 through the end of 2013.

4. Discussion

We describe a 10+ year long, high-resolution simulation which achieves 1/60° horizontal resolution in the Labrador Sea via two nests inside a regional configuration, resolving mesoscale and sub-mesoscale processes which strongly impact the deep convection which occurs here. We show that lower-resolution simulations fail to resolve these key processes that strongly control the production of Labrador Sea Water, an important water mass within the Atlantic Meridional Overturning Circulation. While the NATL60 and eNATL60 simulations were designed with the SWOT altimetry satellite mission in mind (NATL60 website: https://meom-group.github.io/swot-natl60/virtual-ocean.html), their integration period, like many other high-resolution simulations, is a handful of years. LAB60, although covering a much smaller region, could be a valuable asset to many users who require a lengthy period of high-resolution model output. We also have included three passive tracers which are often excluded in simulations at this resolution. Our three passive tracers highlight regions where each water mass enters the interior region of the Labrador Sea, demonstrating the pathways of buoyant Greenland melt and Irminger water. Furthermore, we trace Labrador Sea Water which is formed during the convective winter period.

We show that LAB60 has greater EKE than our lower-resolution simulation, resolving eddy fluxes including Irminger Rings, boundary current eddies, and likely convective eddies as indicated by greater EKE within the interior. Boundary current eddies still appear relatively disconnected from the interior basin, adding further support that these eddies have limited influence on convection and restratification (Rieck et al., 2019). We offer no additional support regarding the relative importance of Irminger Rings and convective eddies on controlling deep convection; this is currently being investigated for a later manuscript. Model drift appears very low, a large improvement over the ANHA4 and ANHA12 configurations. The drift might produce

slightly denser LSW than observations suggest, however LAB60s density is much more accurate than ANHA4 and ANHA12. The boundaries of LAB60, supplied by the inner SPG12 nest, may influence the high-resolution nest. We note that the North Atlantic Current, which is close to the boundary, has less EKE and vorticity than the ANHA4 and ANHA12 simulations. Conversely, the WGC close to the eastern nested boundary has multiple jets which have been noted in hydrographic data (Pickart, personal communication). Boundary communication is always a concern in nested simulations and LAB60 is no different. More investigation will reveal any potential boundary issues but our results so far indicate no further areas of potential concern.

Others have investigated the Labrador Sea using numerical simulations with different resolution. Böning et al. (2016) traced Greenland meltwater with the 1/20° VIKING20 and 1/4° ORCA025 simulations, noting more meltwater entered the interior Labrador Sea at higher resolution partially as a result of greater WGC eddy fluxes but not from the Labrador coast. The minor amount of eddy fluxes from the Labrador coast has been noted earlier even at lower resolution (1/3°; Myers, 2005). Steadily increasing horizontal resolution has so far not changed this for the Labrador coast, though this is opposite for the WGC. LAB60 has a clear increase in EKE and likely greater eddy fluxes from the WGC into the interior of the Labrador Sea.

We have many ambitious research topics which we plan to use LAB60 to investigate. This includes, but is not limited to, the variability and structure of the West Greenland Coastal Current, Labrador Sea Water production, and the role of both Irminger Rings and convective eddies in controlling stratification in the Labrador Sea. This lengthy high-resolution simulation with three passive tracers will provide valuable information for many numerical studies within the Labrador Sea for years to come.

Code and/or data availability

The FORTRAN code used to carry out the LAB60 simulation can be accessed from the NEMO version 3.6 repository (https://forge.ipsl.jussieu.fr/nemo/browser/NEMO/releases/release-3.6). A few FORTRAN files were modified to handle our passive tracers. The complete FORTRAN files as well as the CPP.keys, namelists, and associated files can be found on Zenodo (Pennelly, 2020). Initial and

boundary conditions, atmospheric forcing, and numerical output were too large to host on a repository and instead are hosted on our lab's servers as well as the Compute Canada Niagara server. These data can be requested by emailing the corresponding author.

Author Contribution

PM designed the layout of the LAB60 configuration which included the region of interest, numerical length, and which forcing and initial conditions to supply, as well as supervised CP. CP produced the configuration, modified the FORTRAN code, set up the configuration on the high-performance computing systems, carried out the simulation, and performed the analysis. The manuscript was prepared by CP with contributions by PM.

Acknowledgements

The authors would like to thank the NEMO development team as well as the DRAKKAR group for providing the model code and continuous guidance. We express our thanks to Westgrid and Compute Canada (http://www.computecanada.ca) for the computational resources to carry out our numerical simulations as well as archival of the experiments. We would like to thank Nathan Grivault for his help to migrate our configuration between computing clusters, as well as Charlene Feucher for her help with ARGO data. This work was supported by an NSERC Climate Change and Atmospheric Research Grant (Grant RGPCC 433898) as well as an NSERC Discovery Grant (Grant RGPIN 04357).

The authors declare that they have no conflict of interest.

References

Amante, C. and Eakins, B.W.: ETOPO1 1 Arc-minute global relief model: procedures data sources and analysis. NOAA Technical Memorandum NESDIS, NGDC-24 19, 2009.

Bacon, S., Gould, W.J., and Jia, Y.: Open-ocean convection in the Irminger Sea. Geophysical Research Letters, 30(5), 2003.

Bamber, J., van den Broeke, M., Ettema, J., Lenaerts, J., and Rignot, E.: Recent large increases in freshwater fluxes from Greenland into the North Atlantic. Geophysical Research Letters, 39(19), 2012.

Barnier, B., Madec, G., Penduff, T., Molines, J-M., Treguier, A-M., Le Sommer, J., Beckmann, A., Biastoch, A., Böning, C., Dengg, J., Derval, C., Durand, E., Gulev, S., Remy, R., Talandier, C., Theetten, S., Maltrud, M., Mcclean, J., and De Cuevas, B.: Impact of partial steps and momentum advection schemes in a global ocean circulation model at eddy permitting resolution. Ocean Dynamics, 56 (5-6), 543-567, 2006.

Böning, C.W., Behrens, E., Biastoch, A., Getzlaff, K., and Bamber, J.L.: Emerging impact of Greenland meltwater on deepwater formation in the North Atlantic Ocean. Nature Geoscience, 97(7), 523, 2016.

Brossier, C.L., Léger, L., Giordani, H.,Beuvier, J., Bouin, M.N., Ducrocq, W., and Fourrié, N.: Dense water formation in the north-western Mediterranean area during HyMeX-SOP2 in 1/36° ocean simulations: Ocean-atmosphere coupling impact. Journal of Geophysical Research: Oceans, 122(7), 5749-5773, 2017.

Bryden, H.L., Longworth, H.R., and Cunningham, S.A.: Slowing of the Atlantic meridional overturning circulation at 25°N. Nature, 438(7068), 655, 2005.

Cael, B.B. and Jansen, M.F.: On freshwater fluxes and the Atlantic meridional overturning circulation. Limnology and Oceanography, 5(2), 185-192, 2020.

Chanut, J., Barnier, B., Large, W., Debreu, L., Penduff, T., Molines, J.M., and Mathiot, P.: Mesoscale eddies in the Labrador Sea and their contribution to convection and restratification. Journal of Physical Oceanography, 28(8), 1617-1643, 2008.

Chassignet, E.P. and Xu, X.: Impact of horizontal resolution (1/12 to 1/50) on Gulf Stream separation, penetration, and variability. Journal of Physical Oceanography, 47(8), 1999-2021, 2017.

Courtois, P., Hu, X., Pennelly, C., Spence, P., and Myers, P.G.: Mixed layer depth calculation in deep convection regions in ocean numerical models. Ocean Modelling, 120, 60-78, 2017.

Cuny, J., Rhines, P.B., and Kwok, R.,: Davis Strait volume, freshwater and heat fluxes. Deep Sea Research Part I: Oceanographic Research Papers, 52.3, 519-542, 2005.

Curry, B., Lee, C.M., and Petrie, B.: Volume, freshwater, and heat fluxes through Davis Strait, 2004-05. Journal of Physical Oceanography, 41(3), 429-436, 2011.

Curry, B., Lee, C.M., Petrie, B., Moritz, R.E. and Kwok, R.: Multiyear volume, liquid freshwater, and sea ice transports through Davis Strait, 2004-10. Journal of Physical Oceanography, 44(4), 1244-1266, 2014.

Dai, A., Qian, T., Trenberth, K.E., and Milliman, J.D.: Changes in continental freshwater discharge from 1948 to 2004. Journal of Climate, 22(10), 2773-2792, 2009.

Debreu, L., Vouland, C., and Blayo, E.: AGRIF: Adaptive grid refinement in Fortran. Computers and Geosciences, 34(1), 8-13, 2008.

Dussin, R., Barnier, B., and Brodeau, L.: The making of Drakkar forcing set DFS5, Grenoble, France: LGGE, 2016.

Ferry, N., Parent, L., Garric, G., Barnier, B., and Jourdain, N.C.: Mercator global eddy permitting ocean reanalysis GLORYS1V1: Description and results. Mercator-Ocean Quarterly Newsletter, 36, 15-27, 2010.

Fichefet, T., and Maqueda, M.A.M.: Sensitivity of a global sea ice model to the treatment of ice thermodynamics and dynamics. Journal of Geophysical Research: Oceans, 102(C6), 12609-12646, 1997.

Fischer, J., Visbek, M., Zantopp, R., Nunes, N.: Interannual to decadal variability of outflow from the Labrador Sea. Geophysical Research Letters, 37(24), 2010.

Frajka-Williams, E., Rhines, P.B., and Eriksen, C.C.: Horizontal stratification during deep convection in the Labrador Sea. Journal of Physical Oceanography, 44(1), 220-228, 2014.

Fratantoni, P.S. and Pickart, R.S.: The Western North Atlantic Shelfbreak Current System in Summer. Journal of Physical Oceanography, 37(10), 2509-2533, 2007.

Fresnay, S., Ponte, A.L., Le Gentil, S., Le Sommer, J.: Reconstruction of the 3-D dynamics from surface variable in a high-resolution simulation of the North Atlantic. Journal of Geophysical Research: Oceans, 123(3), 1612-1630, 2018.

Garcia-Quintana, Y., Courtois, P., Hu, X., Pennelly, C., Kieke, D., and Myers, P.G.: Sensitivity of Labrador Sea Water formation to changes in model resolution, atmospheric forcing, and freshwater input. Journal of Geophysical Research: Oceans, 124(3), 2126-2152, 2019.

545 Gelderloos, R., Katsman, C.A. and Drijfhout, S.S.: Assessing the roles of three eddy types in
546 restratifying the Labrador Sea after deep convection. Journal of Physical Oceanography, 41(11),
547 2102-2119, 2011.
548 Gordon, A.L., Visbeck, M., and Comiso, J.C.: A possible link between the Weddell Polynya and
549 the Southern Annular Mode. Journal of Climate, 20(11), 2558-2571, 2007.
550 Hansen, B., and Østerhus, S.: North Atlantic-Nordic Seas exchanges. Progress in Oceanography,
551 45(2), 109-208, 2000.
552 Hátún, H., Eriksen, C.C., and Rhines, P.B.: Buoyant eddies entering the Labrador Sea observed
553 with gliders and altimetry. Journal of Physical Oceanography, 37(12), 2838-2854, 2007.
554 Holte, J., and Talley, L.: A new algorithm for finding mixed layer depths with applications to
555 Argo data and Subantarctic Mode Water formation. Journal of Atmospheric and Oceanic
556 Technology, 26(9), 1920-1939, 2009.
557 Kieke, D., Klein, B., Stramma, L., Rhein, M., and Koltermann, K.P.: Variability and propagation of
558 Labrador Sea Water in the southern subpolar North Atlantic. Deep Sea Research Part I:
559 Oceanographic Research Papers, 56(10), 1656-1674, 2009.
560 Lab Sea Group: The Labrador Sea deep convection experiment. Bulletin of the American
561 Meteorological Society, 79(10), 2033-2058, 1998.
562 Large, W.G., and Yeager, S.G.: The global climatology of an interannually varying air-sea flux
563 data set. Climate Dynamics, 33(2-3), 341-364, 2008
564 Latif, M., Roechner, E., Mikolajewicz, U., and Voss, R.: Tropical stabilization of the thermohaline
565 circulation in a greenhouse warming simulation. Journal of Climate, 13(11), 1809-1813, 2000.
566 Lazier, J., Hendry, R., Clarke, A., Yashayaev, I., and Rhines, P.: Convection and restratification in
567 the Labrador Sea, 1990-2000. Deep Sea Research Part I: Oceanographic Research Papers,
568 49(10), 1819-1835, 2002.
569 Lazier, J.R.N., and Wright, D.G.: Annual velocity variations in the Labrador Current, Journal of
570 Physical Oceanography, 23(4), 659-678, 1993.
571 Lilly, J.M., Rhines, P.B., Visbeck, M., Davis, R., Lazier, J.R.N., Schott, F., and Farmer, D.: Observing
572 deep convection in the Labrador Sea during winter 1994/95. Journal of Physical Oceanography,
573 29, 2065-2098, 1999.

574 Lilly, J.M., Rhines, P.B., Schott, F., Lavender, K., Lazier, J., Send, U., and D'Asaro, E.:
575 Observations of the Labrador Sea eddy field. Progress in Oceanography, 59(1), 75-176, 2003.
576 Lin, P., Pickart, R.S., Torres, D.J., and Pacini, A.: Evolution of the freshwater coastal current at
577 the southern tip of Greenland. Journal of Physical Oceanography, 48(9), 2127-2140. 2018
578 Madec, G.: Note du Pôle de modélisation. Institut Pierre-Simon Laplace (IPSL), France, No 27,
579 ISSN No 1288-1619, 2008.
580 Marshall, J. and Schott, F.: Open-ocean convection: Observations, theory, and models. Reviews
581 of Geophysics, 37(1), 1-64, 1999.
582 Marzocchi, A., Hurshi, J.J.M., Holiday, N.P., Cunningham, S.A., Blaker, A.T., and Coward, A.C.:
583 The North Atlantic subpolar circulation in an eddy-resolving global ocean model. Journal of
584 Marine Systems, 142, 126-143, 2015.
585 McGeehan, I. and Maslowski, W.: Impact of shelf-basin freshwater transport on deep
586 convection in the western Labrador Sea. Journal of Physical Oceanography, 41(11), 2187-2210,
587 2011.
588 Müller, V., Kieke, D., Myers, P.G., Pennelly, C., and Mertens, C.: Temperature flux carried by
589 individual eddies across 47° in the Atlantic Ocean. Journal of Geophysical Research: Oceans,
590 122(3), 2441-2464, 2017.
591 Müller, V., Kieke, D., Myers, P.G., Pennelly, C., Steinfeldt, R., and Stendardo, I.: Heat and
592 freshwater transport by mesoscale eddies in the southern subpolar North Atlantic. Journal of
593 Geophysical Research: Oceans, 124(8), 5565-5585, 2019.
594 Myers, P.: Impact of freshwater from the Canadian Arctic Archipelago on Labrador Sea water
595 formation. Geophysical Research Letters, 32(6), 2005.
596 Pennelly, C.: A 1/60 degree NEMO configuration within the Labrador Sea: LAB60, Zenodo,
597 http://doi.org/10.5281/zenodo.3762748, 2020.
598 Pennelly, C. Hu, X., and Myers, P.G.: Cross-isobath freshwater exchange within the North
599 Atlantic Subpolar Gyre. Journal of Geophysical Research: Oceans, 124(10), 6831-6853, 2019.
600 Rattan, S., Myers, P.G., Treguier, A.M., Theetten, S., Biastoch, A., and Böning, C. Towards an
601 understanding of Labrador Sea salinity drift in eddy-permitting simulations. Ocean Modelling,
602 35(102), 77-88, 2010.

Rieck, J.K., Böning, C.W., and Getzlaff, K.: The nature of eddy kinetic energy in the Labrador Sea: Different types of mesoscale eddies, their temporal variability, and impact on deep convection. Journal of Physical Oceanography, 49(8), 2075-2094, 2019.

Schmidt, S. and Send, U.: Origin and composition of seasonal Labrador Sea freshwater. Journal of Physical Oceanography, 37(6), 1445-1454, 2007.

Schulze, L.M., Pickart, R.S., and Moore, G.W.K.: Atmospheric forcing during active convection in the Labrador Sea and its impact on mixed-layer-depths. Journal of Geophysical Research: Oceans, 121(9), 6978-6992, 2016.

Smith, G.C., Roy, F., Mann, P., Dupont, F., Brasnett, B., Lemieux, J.F., Laroche, S., and Bélair, S.: A new atmospheric dataset for forcing ice-ocean models: Evaluation of reforecasts using the Canadian global deterministic prediction system. Quarterly Journal of the Royal Meteorological Society, 140(680), 881-894, 2014.

Straneo, F.: Heat and freshwater transport through the central Labrador Sea. Journal of Physical Oceanography, 36(4), 606-628, 2006.

Straneo, F. and Saucier, F.: The arctic-subarctic exchange through Hudson Strait. Arctic-Subarctic Ocean Fluxes, Springer, Dordrecht, 249-261, 2008.

De Steur, L., Hansen, E., Gerdes, R., Karcher, M., Fahrbach, E., Holfort, J.: Freshwater fluxes in the East Greenland Current: A decade of observations. Geophysical Research Letters, 36(23), 2009.

Su, Z., Wang, J., Klein, P., Thompson, A.F., and Menemenlis, D.: Ocean submesoscales as a key component of the global heat budget. Nature communications, 9(1), 1-8, 2018.

Tréquier, A.M., Theetten, S., Chassignet, E.P., Penduff, T., Smith, R., Talley, L., Beismann, J.O., and Böning, C.: The North Atlantic subpolar gyre in four high-resolution models. Journal of Physical Oceanography, 35(5), 757-774, 2005.

Yashayaev, I. and Loder, J.W.: Recurrent replenishment of Labrador Sea Water and associated decadal-scale variability. Journal of Geophysical Research: Oceans, 121(11), 8095-8814, 2016.

Yashayaev, I.: Hydrographic changes in the Labrador Sea, 1960-2005. Progress in Oceanography, 73(3-4), 242-276, 2007.

631 Whiteworth, T. and Orsi, A.H.: Antarctic Bottom Water production and export by tides in the
632 Ross Sea. Geophysical Research Letters 33(12), 2006.
633 Zalesak, S.T.: Fully multidimensional flux-corrected transport algorithms for fluids. Journal of
634 computational physics, 31(3), 335-362, 1979.

635

636 Tables

637

638 Table 1: Domain settings for the ANHA4 parent domain, SPG12 and LAB60 nested domains.
639 Other settings which are invariant to the domain are shown in Table 2.

Setting	ANHA4	SPG12	LAB60
Horz. Resolution	1/4°	1/12°	1/60°
X points	544	724	1179
Y points	800	694	2659
Timestep [s]	720	240	48
Horiz. Eddy Viscosity [$m^4 s^{-1}$]	1.5x10^11	1.5x10^10	3.5x10^8
Horiz. Eddy Diffusivity [$m^2 s^{-1}$]	300	50	20
Lateral Slip Conditions	Free slip	Free slip	No slip

640
641
642
643
644
645
646
647
648
649
650
651
652

653 Table 2: Model configuration settings which are identical between all three domains. **Bold**
654 values indicate values which were changed when we migrated LAB60 from the Graham cluster
655 to Niagara.

Configuration Setting		Value
Vertical grid		75 geopotential levels
Sea-ice model		LIM 2 (Fichefet and Maqueda, 1997)
Bulk formula		CORE (Large and Yeager, 2008)
Liquid discharge		Dia et al. (2009) + Bamber (2012: Greenland)
Solid discharge		Input as liquid
Surface Restoring		None
Initial conditions		Glorys1v1 (T,S,U,V,SSH,ice)
Open boundary conditions		Glorys1v1 (T,S,U,V,ice)
Atmospheric forcing:		
	2002-2006	CGRF (Smith et al, 2014)
	2007-2017	Drakkar Forcing Set 5.2 (Dussin et al. 2016)
Lateral momentum		Bilaplacian operator
Lateral diffusion		Laplacian operator
Vertical eddy viscosity		1x10^-4 $m^2 s^{-1}$
Vertical eddy diffusivity		1x10^-5 $m^2 s^{-1}$
Mixed layer scheme		Holte and Talley (2009)
Bottom friction		Nonlinear
Hydrostatic approximation		Yes
Passive tracers		Three (see Figure 2)
CPU requested		672 (**3000**), Broadwell 2.1 GHz (Skylake 2.4 GHz)
Time to complete 1 year		Approximately 700 (**200**) hours
Initialization date		January 1st, 2002

656

657

658 Figures

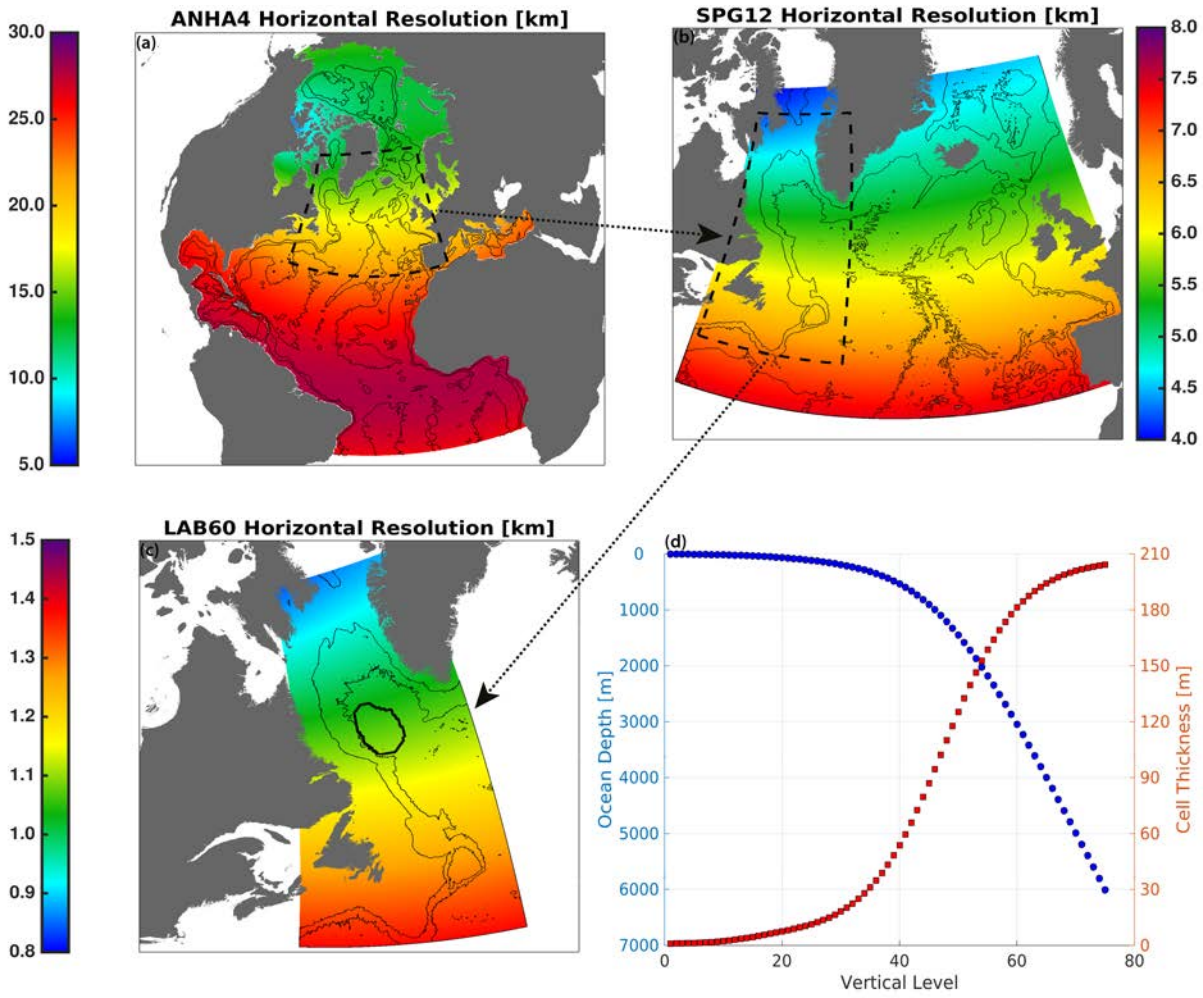

Figure 1: Domain setup for the (a) ANHA4 parent domain, (b) the SPG12 nest, and (c) the LAB60 nest. Horizontal grid resolution, in km, is identified by color. All domains share identical vertical grid structure (d). The thick black contour in (c) identifies a region of interest where calculations of LSW's density, thickness, and mixed layer depth are determined. The 1000m, 3000m, and 5000m isobaths are shown via the thin black contours.

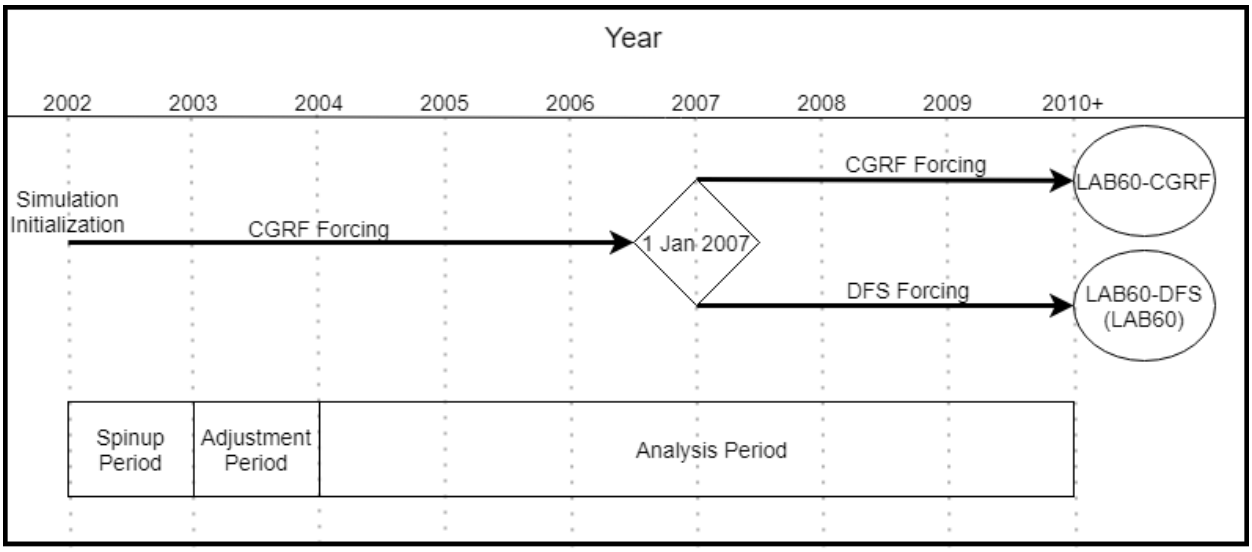

667

668 Figure 2: Diagram showing the multiple periods of the LAB60 simulation. The original simulation
669 was initialized with CGRF atmospheric forcing in 2002, although a branch swapping to DFS
670 occurred at the start of 2007. This DFS branch is what is primarily presented in this study.

671

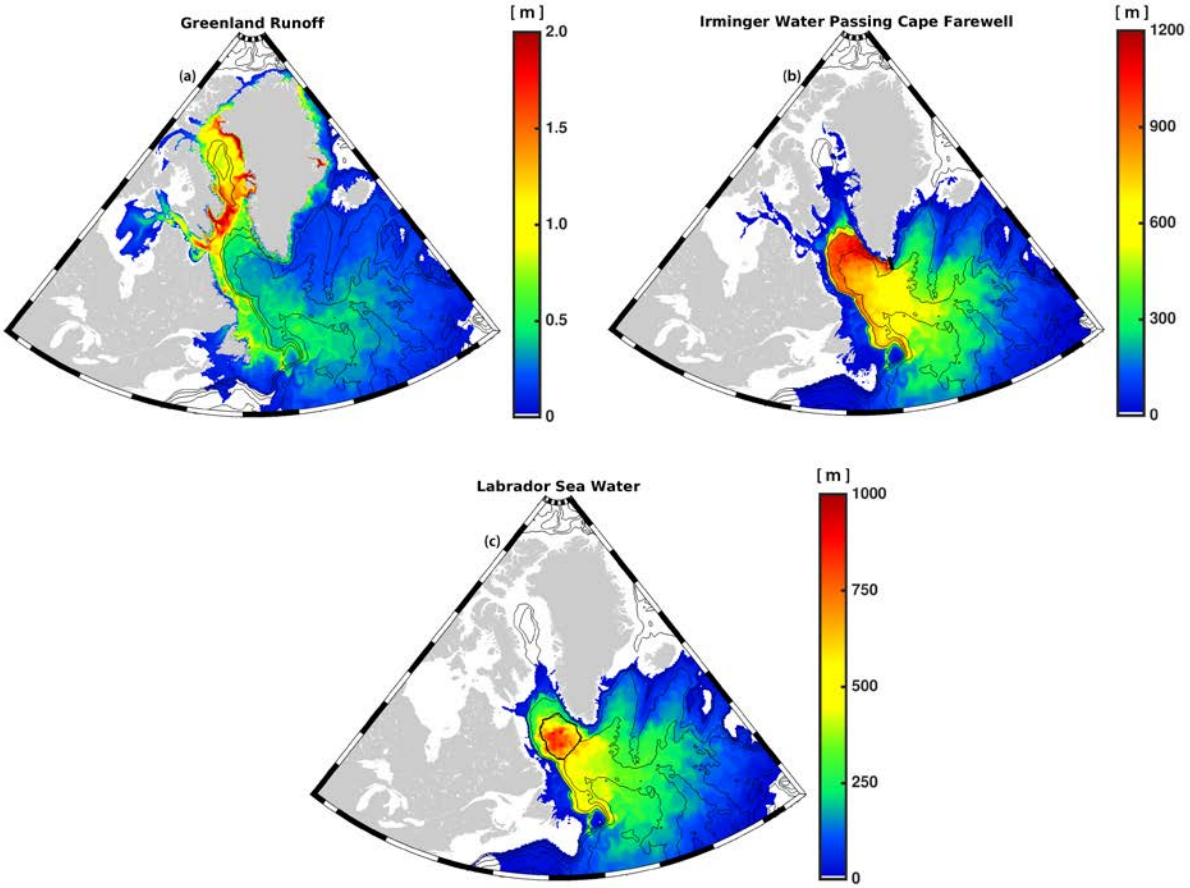

672

673 Figure 3: The three passive tracers used within our LAB60 simulation with source regions
674 indicated by thick black lines: (a) Greenland runoff, (b) Irminger Water (T > 3.5°C, S > 34.88)
675 which flows west past Cape Farwell, and (c) Labrador Sea Water (σ_θ>27.68 kg m^{-3}) produced
676 each convective season. Images are from the simulation date 1 Jan 2010. Bathymetric contours
677 are every 1000m. Units are the thickness, in meters, of the tracer. Note: as all three domains
678 are included in this figure, spatial resolution changes within each subfigure.

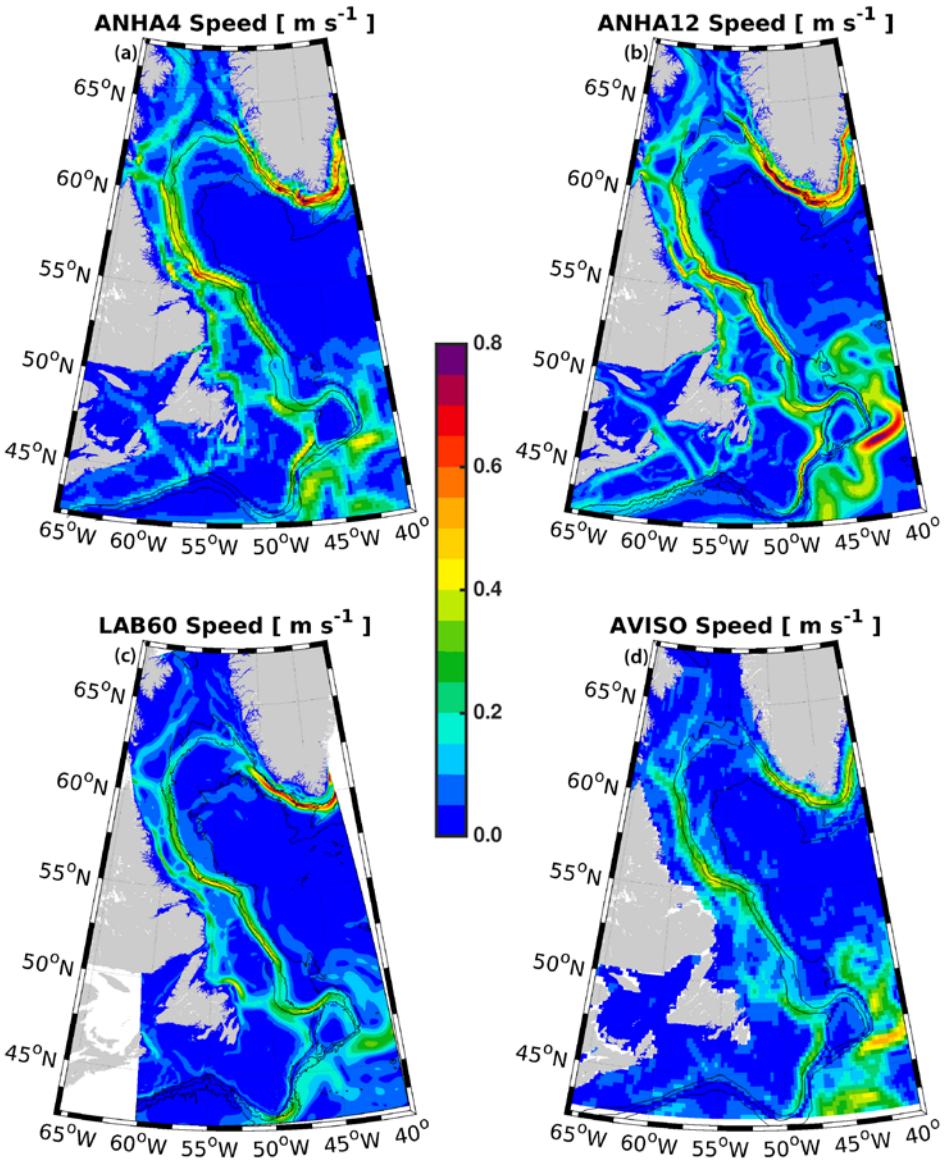

679

680 Figure 4: Top 50m average speed (2004-2013) for the (a) ANHA4, (b) ANHA12, (c) and LAB60
681 simulations, as well as (d) from AVISO observations. The 1000, 2000, and 3000m isobaths are
682 shown by the black contour lines.

683

684

685

686

687

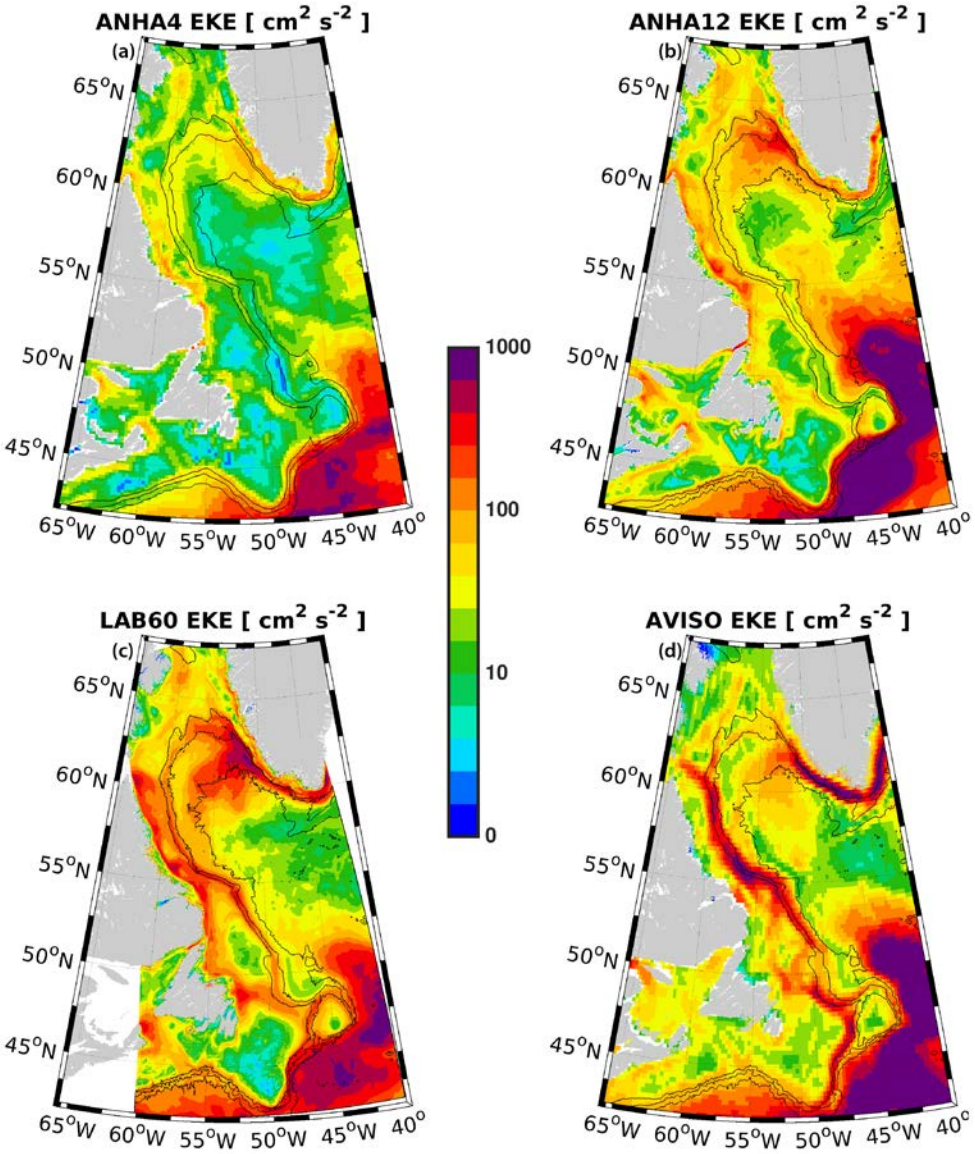

688

689 Figure 5: Eddy kinetic energy (EKE), as calculated from geostrophic velocities resulting from the
690 sea level height anomaly, are shown for (a) ANHA4, (b) ANHA12, and (c) our LAB60 simulation,
691 from 2004 to 2013. Observations via AVISO are identified in (d). The 1000m, 2000m, and 3000m
692 isobaths are shown by the black contour lines. A log scale was used for clarity.

693

694

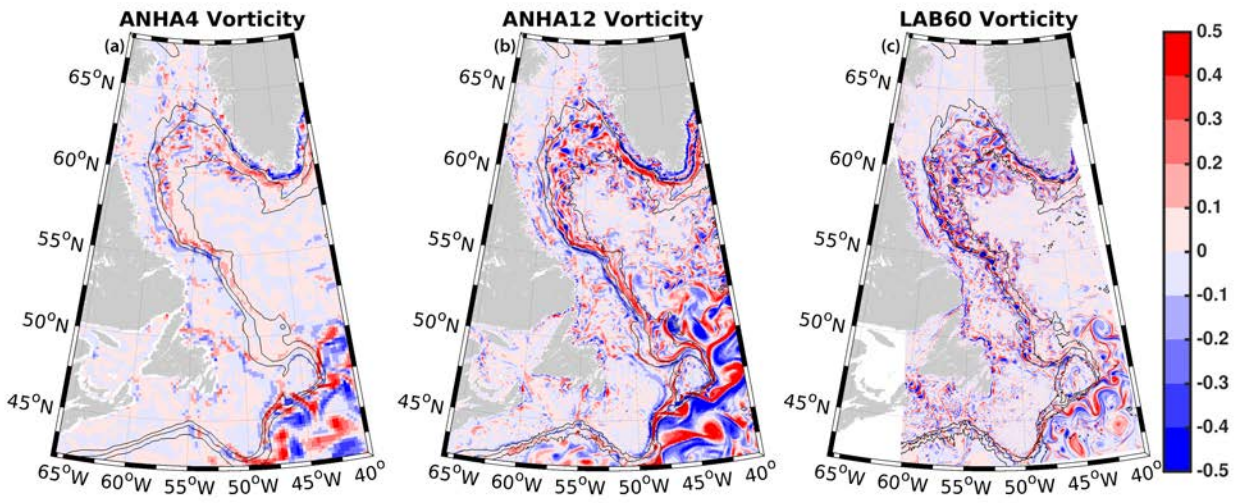

Figure 6: Top 50m relative vorticity, normalized by the planetary vorticity, as simulated by (a) ANHA4, (b) ANHA12, and (c) LAB60 on 16 March 2008. The 1000m, 2000m, and 3000m isobaths are shown by the black contour lines.

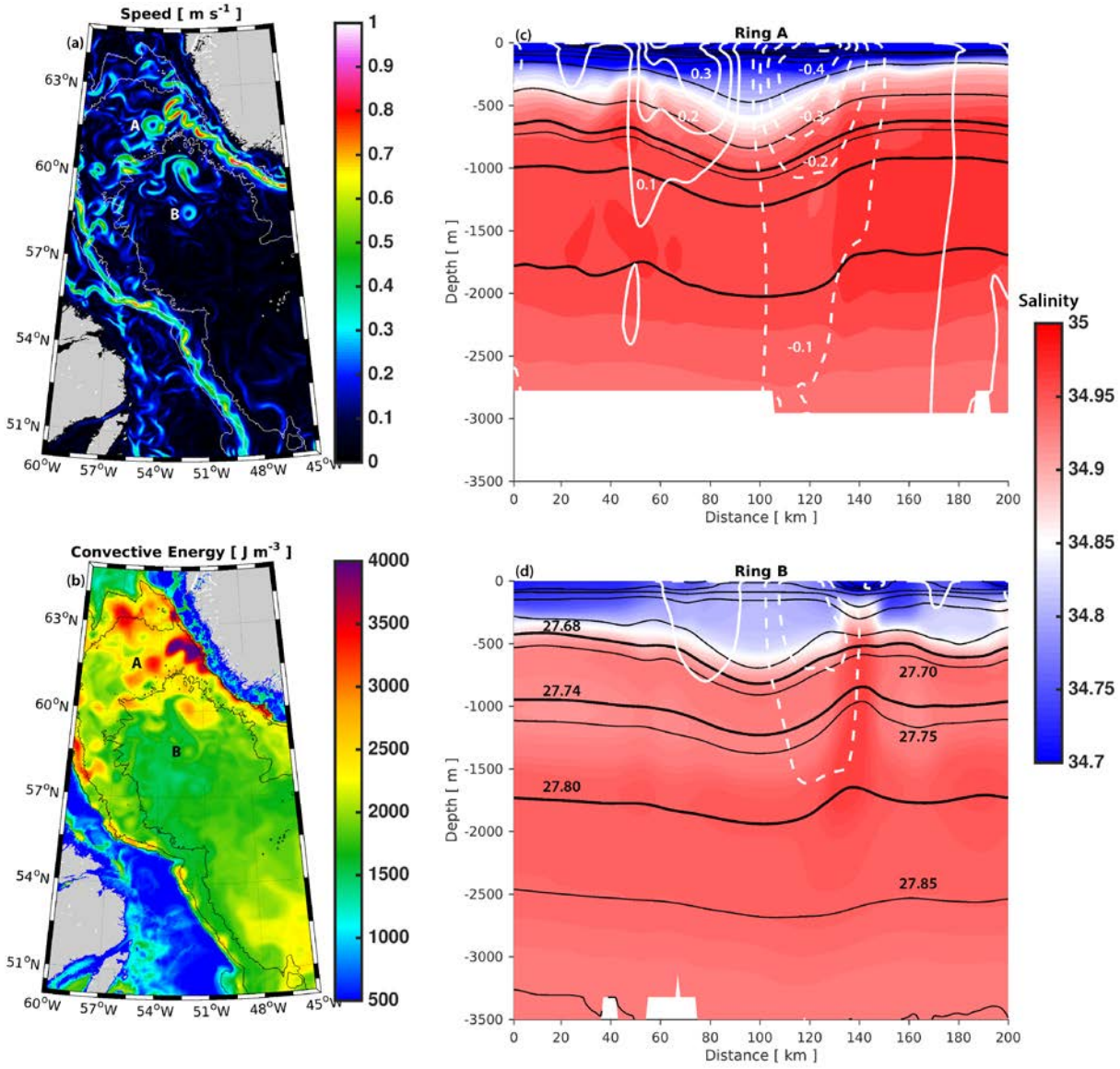

Figure 7: LAB60 snapshot (26 July 2007) of the surface speed (a) and convective energy (b) within the Labrador Sea. Two Irminger Rings are identified by their age with letters: Ring A is a young Irminger Ring, while Ring B is comparatively older. An east-west cross section through each of these Irminger Rings is shown in (c) and (d) where colors indicate salinity, black contours indicate potential density using a contour interval of 0.05 kg m^{-3}, and white contours indicate meridional velocity where southern flow is dashed and northern flow is solid, using a contour interval of 0.1 m s^{-1}. Thick black contours indicate the potential density classification of Upper Labrador Sea Water (σ_θ=27.68 to 27.74 kg m^{-3}) and Classical Labrador Sea Water (σ_θ= 27.74 to 27.80 kg m^{-3}).

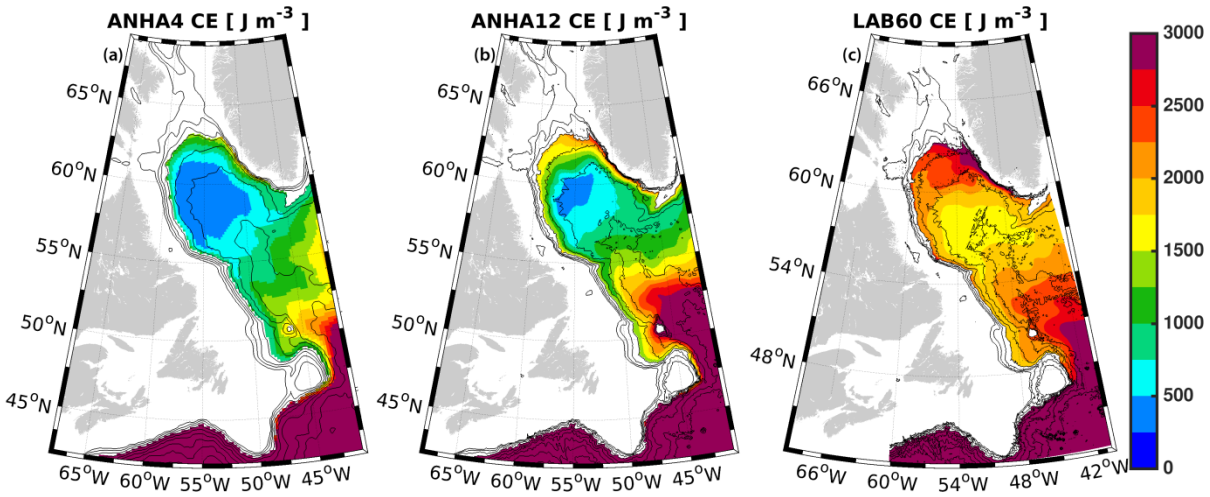

710

711 Figure 8: Convective energy (CE), the strength of stratification down to a reference depth of
712 2000m, is shown for (a) ANHA4, (b) ANHA12, and (c) LAB60. Convective energy was averaged
713 from 2004 through 2013. Values where the depth of the seafloor was less than 2000m were
714 removed to preserve clarity. Bathymetric contours (black lines) are shown every 500m.

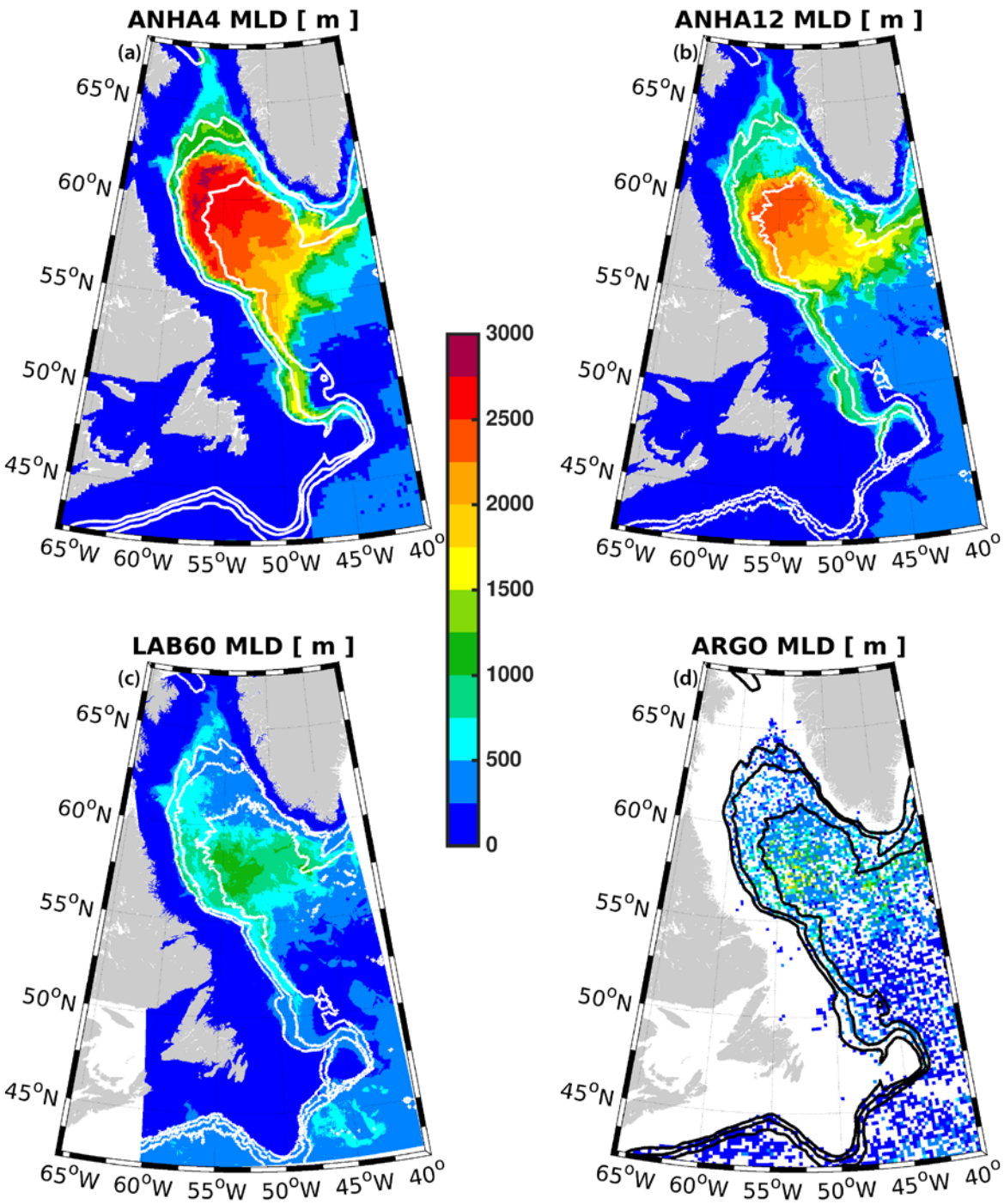

715

716 Figure 9: Maximum mixed layer depth for (a) ANHA4, (b) ANHA12, (c) LAB60, as well as (d)
717 ARGO observations, where available, from 2004 through the end of 2013. For clarity, the ARGO
718 data were placed on the same grid as ANHA4. The 1000m, 2000m, and 3000m isobaths are
719 shown via the white and black contours

720

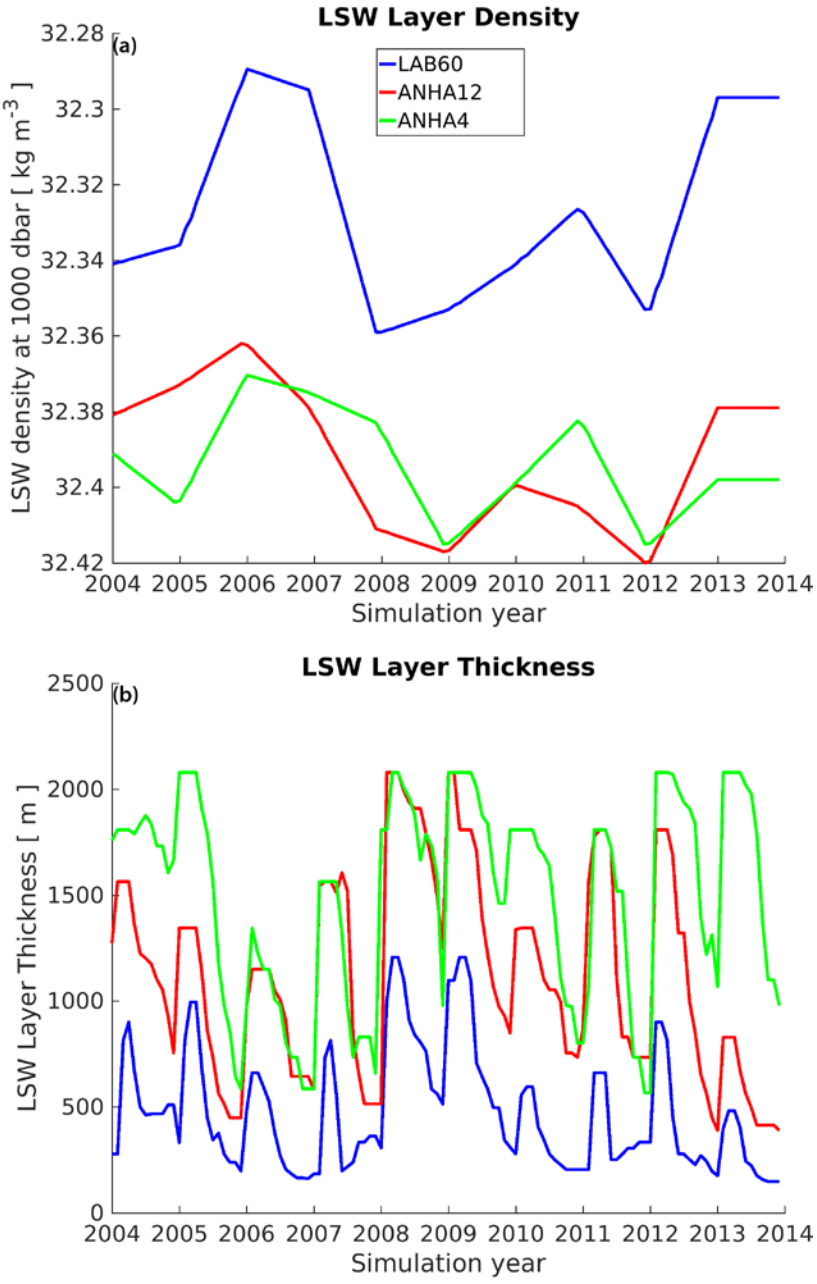

721

722 Figure 10: Labrador Sea Water (LSW) density (a) and thickness (b) for the LAB60, ANHA12, and
723 ANHA4 configurations. LSW density was determined from the thickest layer where a 0.001 kg
724 m^{-3} change in potential density (ref: 1000 dbar) occurred within the black polygon outlines in
725 Fig 1c. The LSW layer was then calculated between this density and one which was 0.02 kg m^{-3}
726 less dense.

727

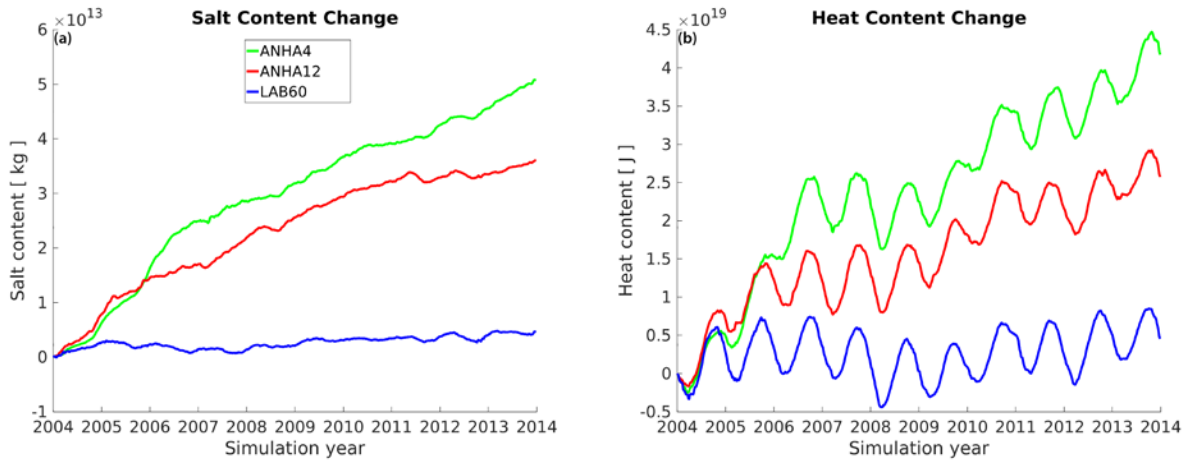

728

729 Figure 11: Numerical salt (a) and heat (b) drift in our three simulations as they evolve since 1
730 Jan 2004. Salt and heat content is calculated over the full ocean column within the polygon in
731 Fig. 1c.

732

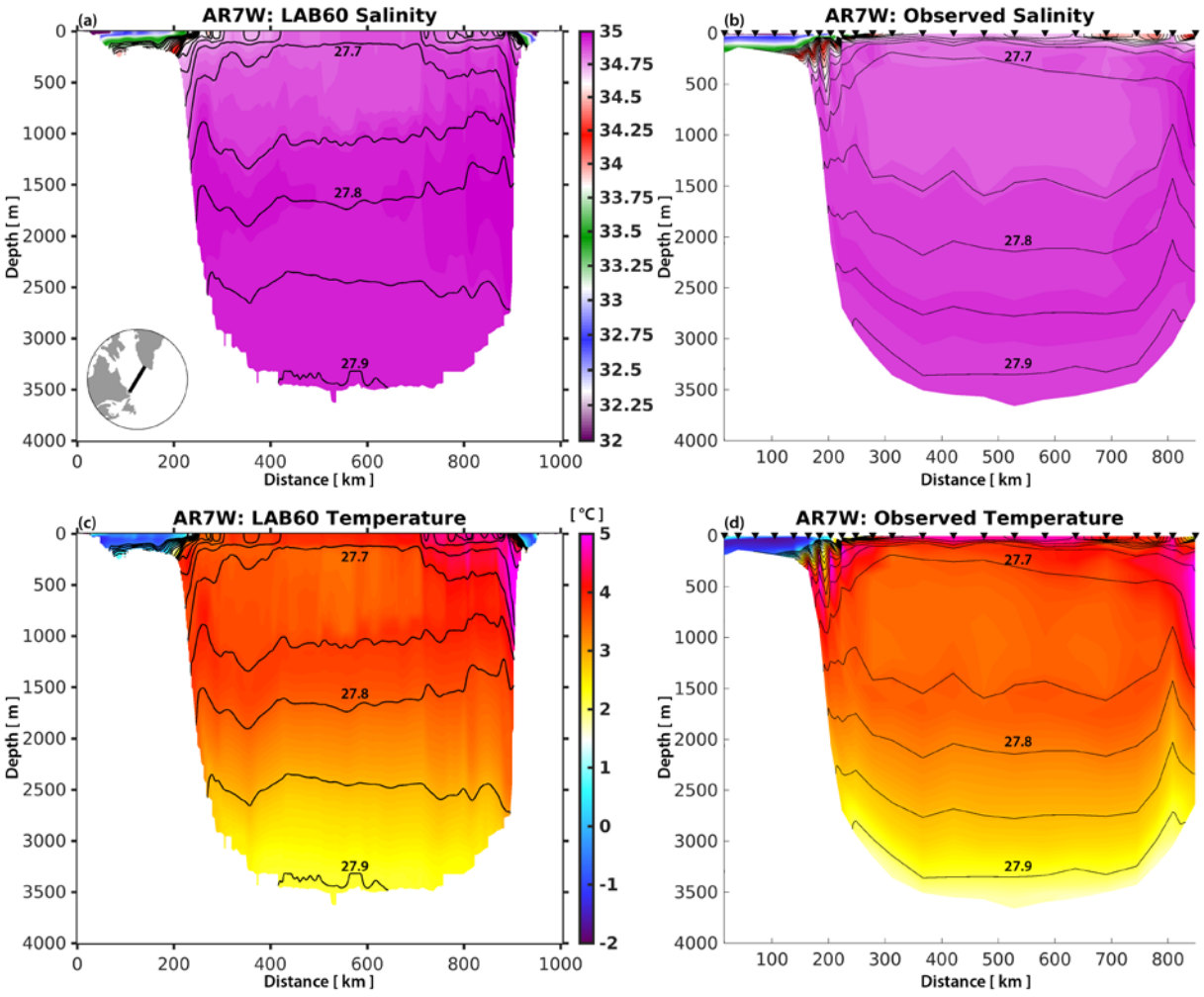

Figure 12: Salinity (top) and temperature (bottom) section across AR7W as determined by the LAB60 simulation (left) and observations (right) from May 2008. Downward triangles identify collection sites across the AR7W transit carried out by the CCGS Hudson. Potential density (black contours) isopycnal interval is 0.05 kg m^{-3}.